



OPEN Renal phenotyping in a hypomorphic murine model of propionic aciduria reveals common pathomechanisms in organic acidurias

Anke Schumann^{1✉}, Ainhoa Martinez-Pizarro², Eva Richard², Christoph Schell³, Anna Laura Kössinger³, Karina A. Zeyer¹, Stefan Tholen³, Oliver Schilling³, Michael Barry⁴, Björn Neubauer⁵, Michael Köttgen^{5,6}, Luciana Hannibal⁷, Lourdes R. Desviat² & Ute Spiekerkötter¹

Mutations in the mitochondrial enzyme propionyl-CoA carboxylase (PCC) cause propionic aciduria (PA). Chronic kidney disease (CKD) is a known long-term complication. However, good metabolic control and standard therapy fail to prevent CKD. The pathophysiological mechanisms of CKD are unclear. We investigated the renal phenotype of a hypomorphic murine PA model (*Pcca*^{-/-}(A138T)) to identify CKD-driving mechanisms. *Pcca*^{-/-}(A138T) mice show elevated retention parameters and express markers of kidney damage progressing with time. Morphological assessment of the *Pcca*^{-/-}(A138T) mouse kidneys indicated partial flattening of tubular epithelial cells and focal tubular-cystic dilation. We observed altered renal mitochondrial ultrastructure and mechanisms acting against oxidative stress were active. LC-MS/MS analysis confirmed disease-specific metabolic signatures and revealed disturbances in mitochondrial energy generation via the TCA cycle. Our investigations revealed altered mitochondrial networks shifted towards fission and a marked reduction of mitophagy. We observed a steep reduction of PGC-1- α , the key mediator modulating mitochondrial functions and a counter actor of mitochondrial fission. Our results suggest that impairment of mitochondrial homeostasis and quality control are involved in CKD development in PA. Therapeutic targeting of the identified pathways might help to ameliorate CKD in addition to the current treatment strategies.

Keywords Propionic aciduria, Mitochondrial dysfunction, Mitochondrial homeostasis, Mitochondrial fission, Chronic kidney disease, Mitochondrial energy metabolism, Mitochondrial quality control

Propionic aciduria (PA, OMIM # 606054) is caused by mutations in the mitochondrial enzyme propionyl-CoA carboxylase (PCC) which catalyzes the final steps of propionate metabolism. Elevated concentrations of propionylcarnitine (C3), 3-OH propionate and methylcitrate are biochemical hallmarks and may have toxic and signaling properties¹. Despite ubiquitous PCC expression, long-term complications include cardiac and neurological impairment as well as chronic kidney disease (CKD), which points towards tissue-specific vulnerability.

¹Department of General Paediatrics, Adolescent Medicine and Neonatology, Faculty of Medicine, Medical Center, University of Freiburg, Breisacherstr. 62, 79106 Freiburg, Germany. ²Centro de Biología Molecular Severo Ochoa, UAM-CSIC, CIBERER, IdiPaz, IUBM, Universidad Autónoma de Madrid, Madrid, Spain. ³Faculty of Medicine, Medical Center, University of Freiburg, Institute for Surgical Pathology, Freiburg, Germany. ⁴Department of Medicine, Division of Infectious Diseases, Mayo Clinic, Rochester, MN 55905, USA. ⁵Department of Medicine IV - Nephrology and Primary Care, Faculty of Medicine and Medical Center, University of Freiburg, Freiburg, Germany. ⁶CIBSS - Centre for Integrative Biological Signaling Studies, University of Freiburg, Freiburg, Germany. ⁷Department of General Paediatrics, Adolescent Medicine and Neonatology, Laboratory of Clinical Biochemistry and Metabolism, Faculty of Medicine, Medical Center, University of Freiburg, Freiburg, Germany. ✉email: anke.schumann@uniklinik-freiburg.de

Studies on the natural history of CKD in PA are scarce but highlight that CKD in PA occurs already in childhood^{2,3} and 50% of adult patients have a GFR of < 60 mL/min⁴. CKD in PA lacks a characteristic renal pattern and standard diagnostic markers like creatinine are poor predictors for onset and follow-up due to decreased muscle mass and low protein diet in PA patients¹. A kidney biopsy in an adult PA patient revealed flattened tubular epithelium and cystic structures with mild focal lymphocytic inflammatory infiltrates⁵. Neither good adherence to diet nor liver transplantation prevents kidney function decline in PA^{2,3}. CKD is a highly relevant but mechanistically not understood complication of PA.

Of note, CKD is a long-known complication in closely related methylmalonic aciduria (MMA), an organic aciduria (OA) presenting with severe and early onset CKD inevitably leading to end stage renal disease⁶. Methylmalonyl-CoA mutase lies two steps downstream of PCC. The metabolic profile is similar with the exception of high concentrations of methylmalonic acid. MMA is associated with tubulointerstitial nephritis and renal tubular acidosis¹. The identification of similarities and differences in these metabolically closely related yet in terms of CKD severity different OAs might be helpful to untangle the underlying mechanisms.

Recently, different studies shed new light on potential CKD driving mechanisms in OAs. Our group and others^{7–9} identified mitochondrial alterations and oxidative stress (ROS) as potential disease driving mechanisms in both OAs. Gallego-Villar et al¹⁰ reported elevated ROS levels in PA patients' fibroblasts and in different organs (brain, muscle, heart, liver) of the *Pcca*^{-/-}(A138T) mouse model, and detected decreased oxidative phosphorylation (OXPHOS) capacity. Measurements of respiratory chain activity in the tissues of both PA and MMA patients showed relevant deficiencies¹¹. The interference of toxic metabolites targeting mitochondrial proteins and leading to energetic dysfunction have been discussed for both entities¹². Different renal MMA models revealed disturbance of mitochondrial homeostasis and mitochondrial quality control (MQC)¹³. Investigation of a renal epithelial cellular model for PA pointed in a similar direction. Cellular stress induced by high protein load aggravated the phenotype⁸. Involvement of posttranslational modification mechanisms like lysine acylation and methylmalonylation might explain altered enzymatic expression patterns and concomitantly function of distinct metabolic pathways^{12,14}.

Comprehensive phenotypic examination and in depth molecular and metabolic profiling in tissue specific models are needed to better understand and treat CKD driving mechanisms in PA, particularly since human kidney is not easily accessible.

In this study, we explored potential CKD driving pathomechanisms in the hypomorphic *Pcca*^{-/-}(A138T) mouse model. We hypothesized that OAs presenting with a renal phenotype might share specific patterns, which can be directly targeted in the future. In line with previous findings for PA and MMA, mitochondrial networks were abnormal in *Pcca*^{-/-}(A138T) mice, while mechanisms counteracting ROS were active. We identified severe disturbances of mitochondrial homeostasis and dynamics while MQC was dysfunctional. The study highlights the role of the mitochondrion for CKD progression in PA and supports the idea that therapies targeting mitochondrial homeostasis might be renoprotective in OAs.

Results

Altered renal and mitochondrial function in *Pcca*^{-/-}(A138T) mice

We investigated serum levels, kidney lysates and sections of wild-type (WT) and *Pcca*^{-/-}(A138T) mice at different time points. We performed our study on female mice, since male mice had a less pronounced renal phenotype (data not shown). LC-MS/MS revealed elevated creatinine levels in *Pcca*^{-/-}(A138T) mice (2.5-fold) as compared to WT (Fig. 1A). The investigation of blood urea nitrogen (BUN) levels in the serum of *Pcca*^{-/-}(A138T) mice showed an increase with time (Fig. 1B). RT-qPCR detected elevated transcription levels of Lipocalin2 (*LCN2*; *Lcn2*) and Kidney injury molecule-1 (*KIM-1*; *Havcr1*) indicating kidney damage (Fig. 1C,D) progressing over time.

The ratios of reduced to oxidized glutathione and cysteine were reduced pointing to a compromised antioxidant system (Fig. 2A). Our study revealed elevated transcription levels of FGF21 (*Fgf21*) in *Pcca*^{-/-}(A138T) mice which supports mitochondrial dysfunction (Fig. 2B). Electron microscopy revealed an extended, filamentous mitochondrial network with mainly preserved cristae structure in WT mice. In contrast, the mitochondrial network was patchy in proximal and distal tubules of the *Pcca*^{-/-}(A138T) model and showed disorganized, rarified networks suggesting structural alterations (Fig. 2C).

Morphological assessment *Pcca*^{-/-}(A138T) mouse kidneys

We performed immuno-histological studies on mouse kidneys at 10 and 23 weeks of age (Fig. 3). Morphological assessment of *Pcca*^{-/-}(A138T) mouse kidneys showed a partial flattening of tubular epithelial cells and focal tubular-cystic dilation (Fig. 3). In some proximal tubular segments, we detected cytoplasmic vacuolization in *Pcca*^{-/-}(A138T) mice. Fibrotic fibers or signs of inflammation were not identified (Fig. 3). Cellular proliferation was comparable in WT and *Pcca*^{-/-}(A138T) mice. Employing SFOG staining (acid-fuchsin, orange-G, anilin-blue), no pronounced accumulation of extracellular matrix was detectable in WT and *Pcca*^{-/-}(A138T) animals.

Metabolic profiling of *Pcca*^{-/-}(A138T) mouse kidneys

We used LC-MS/MS to measure disease-specific markers and tricarboxylic acid cycle (TCA) intermediates in WT and *Pcca*^{-/-}(A138T) mouse kidneys. While lactate levels remained normal, methylcitrate concentrations were excessively elevated (34-fold, Fig. S1A). Propionate concentrations remained unchanged in *Pcca*^{-/-}(A138T) mouse kidneys. MMA concentrations were in tendency higher (Fig. S1A).

α -ketoglutarate is a TCA cycle intermediate involved in nitrogen metabolism and -via conversion to succinyl-CoA- in ATP production. We detected an increase in both α -ketoglutarate (1.8-fold) and succinate (twofold) concentrations (Fig. S1B) in *Pcca*^{-/-}(A138T) mouse kidneys. Malate concentrations were elevated likewise (twofold, Fig. S1B). Both metabolites are linked via the α -ketoglutarate-malate carrier and provide the

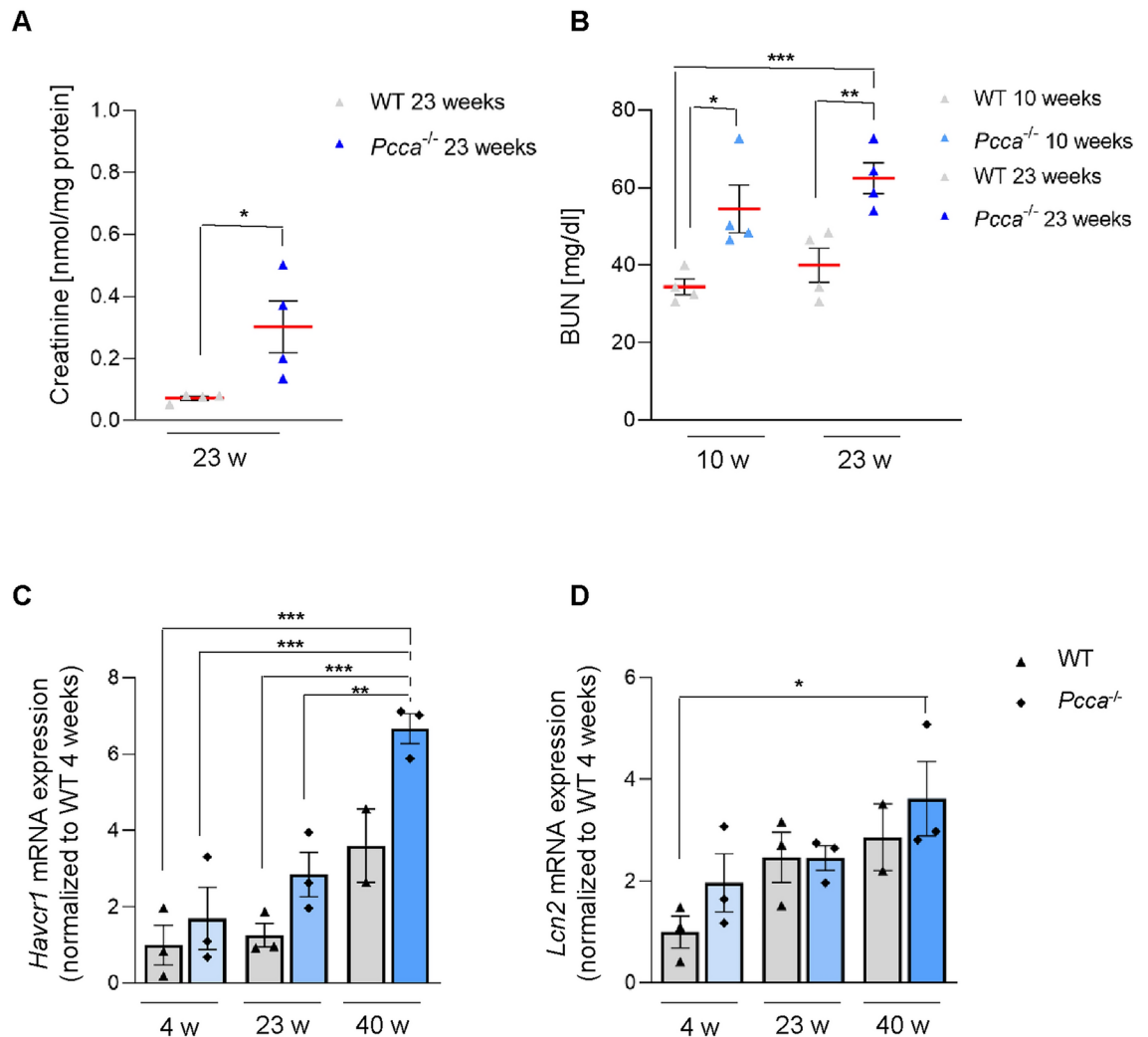


Fig. 1. Kidney disease in *Pcca*^{-/-}(A138T) mice. **(A)** LC–MS/MS quantification of creatinine concentrations in 23-week-old WT and *Pcca*^{-/-}(A138T) mouse kidneys. Creatinine concentration in nmol/mg protein. *n* = 4 per group. **(B)** Blood urea nitrogen (BUN) concentration in the serum of 10- and 23-week-old WT and *Pcca*^{-/-}(A138T) mice. BUN concentration in mg/dl. *n* = 4 per group. **(C)** Transcript levels of kidney injury molecule-1 (KIM-1, *Havcr1*) and lipocalin 2 (LCN2, *Lcn2*) obtained by RT-qPCR in kidney extracts of 4-, 23- and 40-week-old (w) WT and *Pcca*^{-/-}(A138T) mice. *n* = 3 per group, *n* = 2 for WT 40-week-old mice.

respiratory chain (RC) with NADH for ATP synthesis and NAD⁺ regeneration¹⁵. Malonate and itaconate are competitive inhibitors of succinate dehydrogenase (SDH), which is part of both the TCA cycle and the complex II¹⁶. Malonate and itaconate concentrations were elevated (1.7-fold and twofold (Fig. S1B)). Citrate is taken up from the circulation and largely contributes to energy generation via the renal TCA cycle¹⁷. We detected a tendency to higher citrate concentrations (1.7-fold) in the kidneys of *Pcca*^{-/-}(A138T) mice (Fig. S1B).

We used acylcarnitine profiling as indirect read-out for fatty acid oxidation (FAO)¹⁸. Levels of free carnitine were comparable in WT and *Pcca*^{-/-}(A138T) mice (Fig. S1C). Propionyl-carnitine concentrations (C3) were highly elevated in the PA mouse model (8.6-fold, Fig. S1C). Short-chain acylcarnitines were in tendency reduced, while medium- (MC) and long-chain (LC) were equally distributed (Fig. S1C). However, we observed a tendency towards accumulation of C8 and C10 acylcarnitines in *Pcca*^{-/-}(A138T) mice (Fig. S1D).

The concentrations of the disease-associated amino acids glycine, isoleucine, methionine, valine and threonine remained unchanged (Fig. S2A) in *Pcca*^{-/-}(A138T) mice. The ratio of alanine:lysine was markedly reduced, while the ratio of alanine:phenylalanine + tyrosine was comparable in WT and *Pcca*^{-/-}(A138T) mice (Fig. S2B). Amino acid profiling revealed a steep increase of serine concentration (Fig. S2C). A reduction in the alanine:lysine ratio and elevated serine levels have been used as biomarkers for PA^{19,20}.

Regulation of mitochondrial mass and biogenesis in *Pcca*^{-/-}(A138T) mouse kidneys

Kidneys are highly energy dependent organs due to filtration and reabsorption processes. We performed immunoblotting of the mitochondrial marker proteins voltage gated anion channel (VDAC1) and cytochrome c oxidase (COX IV) to evaluate potential mitochondrial adaption mechanisms. We observed an up-regulation of COX IV

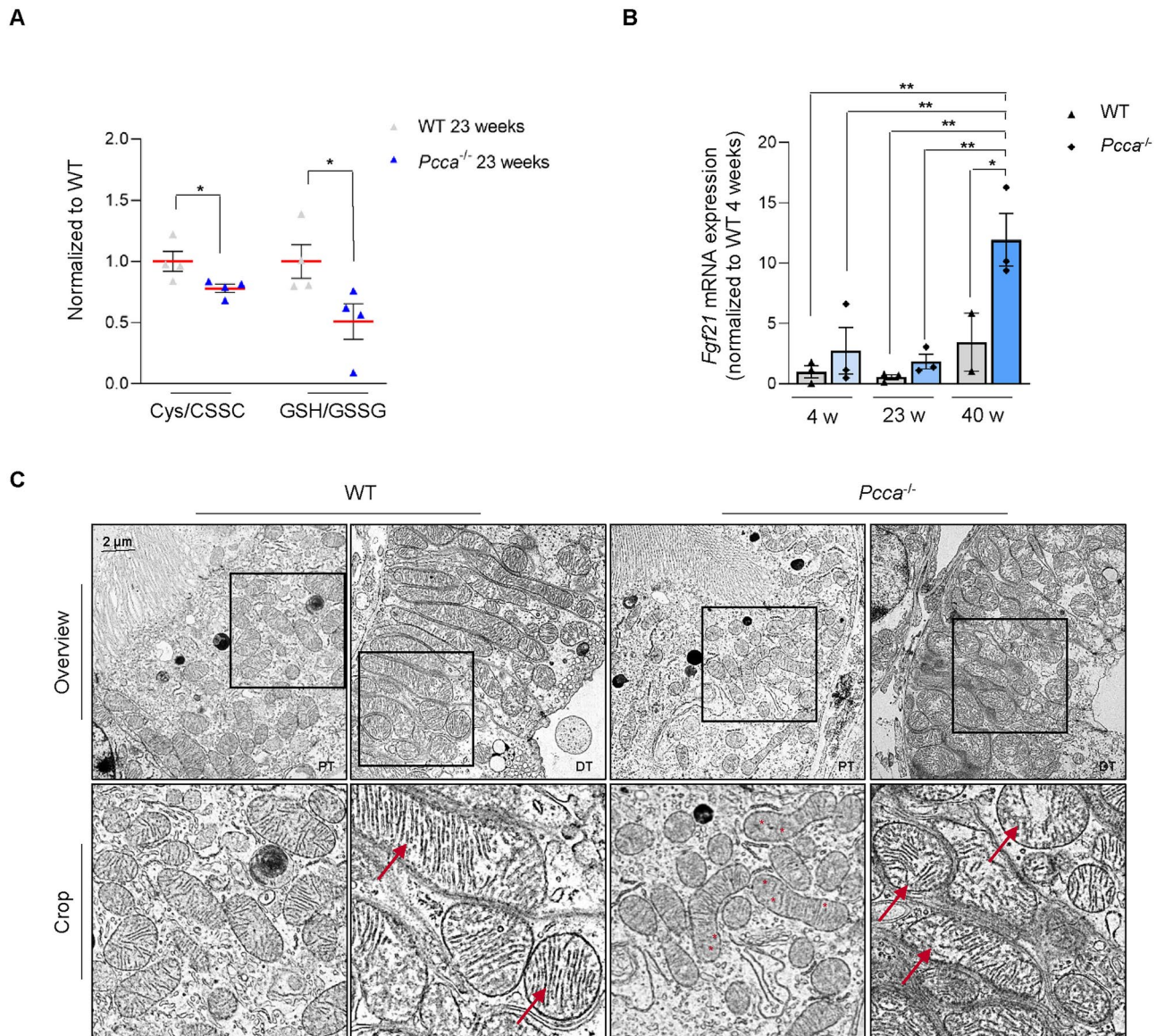


Fig. 2. Altered mitochondrial morphology and function in *Pcca*^{-/-}(A138T) mouse kidneys. **(A)** Quantitative LC-MS/MS analysis ratio of reduced (cysteine) to oxidized (CSSC) of cysteine and reduced (GSH) to oxidized (GSSG) levels of glutathione. Data normalized to WT. n = 4 per group. **(B)** Transcript levels of fibroblast growth factor 2 (FGF21, *Fgf21*) obtained by RT-qPCR in kidney extracts of 4-, 23- and 40-week-old (w) WT and *Pcca*^{-/-}(A138T) mice. n = 3 per group, n = 2 for WT 40-week-old mice. **(C)** Representative transmission electron microscopy of proximal (PT) and distal tubular (DT) segments of 40-week-old WT and *Pcca*^{-/-}(A138T) mouse kidneys (n = 2). Scale bar: 2 μ m. n = 2 per group.

protein expression in the kidneys of 10- and 23-week old *Pcca*^{-/-}(A138T) mice (1.6 and 1.8-fold) compared to WT littermates. Age did not affect VDAC1 and COX IV protein expression (Fig. 4A,B). Peroxisome proliferator-activated receptor-gamma coactivator (PGC-1 α) is the master regulator of mitochondrial biogenesis. PGC-1 α expression was markedly reduced (0.7-fold) in the kidneys of 10-week-old *Pcca*^{-/-}(A138T) mice and slightly further reduced in 23-week-old littermates (Fig. 4A,B). The investigation of additional mitochondrial markers for different mitochondrial compartments by RT-qPCR (inner membrane: succinate dehydrogenase (*Sdh*), intermembrane space: cytochrome c (*Cyts*)) and matrix (pyruvate dehydrogenase subunit alpha (*Pdh1*); Fig. S3A-C)) showed comparable profiles of 4- and 23-week old animals, while 40-week-old WT mice showed a significant up-regulation of these mitochondrial transcripts.

Alterations in mitochondrial dynamics and quality control

Mitochondrial networks constantly undergo coordinated reshaping to sustain ATP production and maintain cellular function, a process called “mitochondrial dynamics”²¹. Mitochondrial dynamics involves fission and fusion processes which are coordinated by the respective marker proteins dynamin related protein (Drp1, fission)

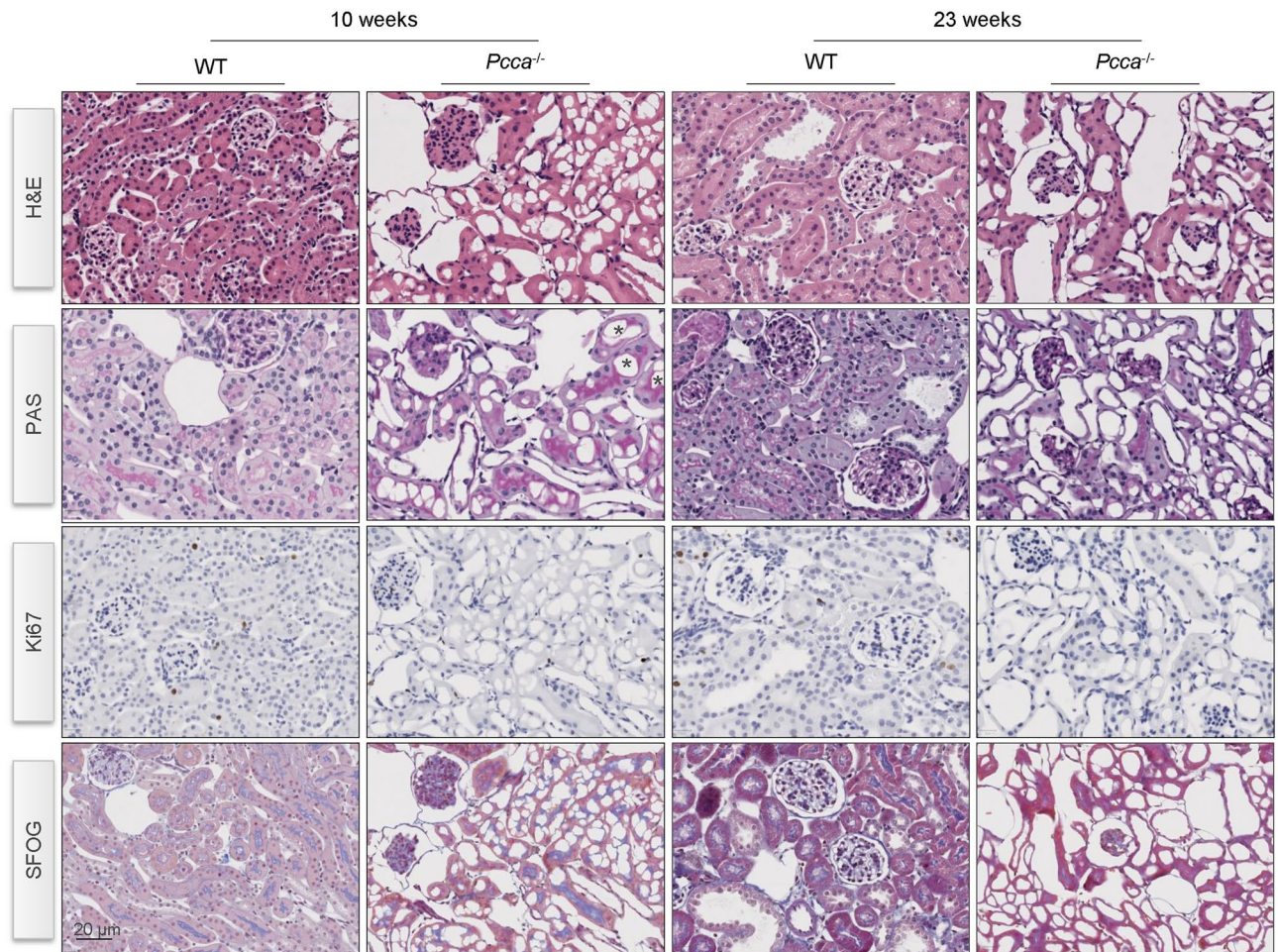


Fig. 3. Partial flattening and focal tubular-cystic dilation in tubular cells of *Pcca*^{-/-} (*A138T*) mice. Immunostaining in kidneys of WT and *Pcca*^{-/-} (*A138T*) mice at 10 and 23 weeks of age addressing tissue structure and proliferation. H&E: hematoxylin and eosin staining; PAS: Periodic acid-Schiff staining; Ki67: Marker of proliferation Ki67; SFOG-staining: acid-fuchsin, orange-G, and aniline-blue staining. Representative images of *n* = 3 mice/group. Scale bar: 20 μ m.

and dynamin-related guanosine triphosphatase coded by the *OPA1* gene as well as mitofusin 1/2 (*Mfn1/2*, fusion)²². Immuno-blotting revealed a strong tendency to mitochondrial fission as evidenced by elevated Drp1 levels (threefold) in kidney lysates of *Pcca*^{-/-} (*A138T*) animals, while the expression of the mitochondrial fusion proteins OPA1 (0.4-fold) and *Mfn1/2* (0.5-fold) was markedly reduced (Fig. 4A,C) compared to WT mice. Again, aging did not aggravate the phenotype on protein level.

Having identified perturbations in mitochondrial dynamics and energy metabolism, we investigated the MQC system. Mitophagy is initiated by PTEN-induced kinase 1 (PINK1)²¹, and in times of mitochondrial stress and membrane depolarization, this protein is no longer cleaved but appears in large amounts on the surface priming mitochondria for degradation. SQSTM1 is a scaffold protein involved in activation of autophagy, a degradative cellular housekeeping pathway involved in cellular stress response²³.

We detected markedly reduced levels (0.3- and 0.5-fold) for PINK1 in the kidneys of *Pcca*^{-/-} (*A138T*) mice (Fig. 4A,D). General autophagy on the other hand was highly active as evidenced by up-regulation of SQSTM1 levels (2- and 2.7-fold, Fig. 4A,D) pointing at a need to compensate for defective mitochondrial clearance. NAD dependent deacetylase 1 (SIRT1) was up-regulated (up to 15-fold) in kidneys of *Pcca*^{-/-} (*A138T*) mice (Fig. 4A,D).

Discussion

The preservation of mitochondrial homeostasis and MQC are essential for energy dependent organs like the kidney²⁴. Deficiency of mitochondrial PCC leads to ROS development in different tissues¹¹ and accumulation of specific potentially toxic metabolites¹. Recently, dysregulation of MQC and altered mitochondrial homeostasis were implicated in CKD development in OAs due to methylmalonyl-CoA mutase deficiency (MMA)^{13,25}.

This study is the first providing insight into renal pathophysiology in a hypomorphic mouse model for PA. Our results suggest that renal involvement in OAs shares indeed common pathomechanisms. PCC deficiency leads to renal mitochondrial dysfunction and metabolic switches in energy metabolism. We detected unbalanced

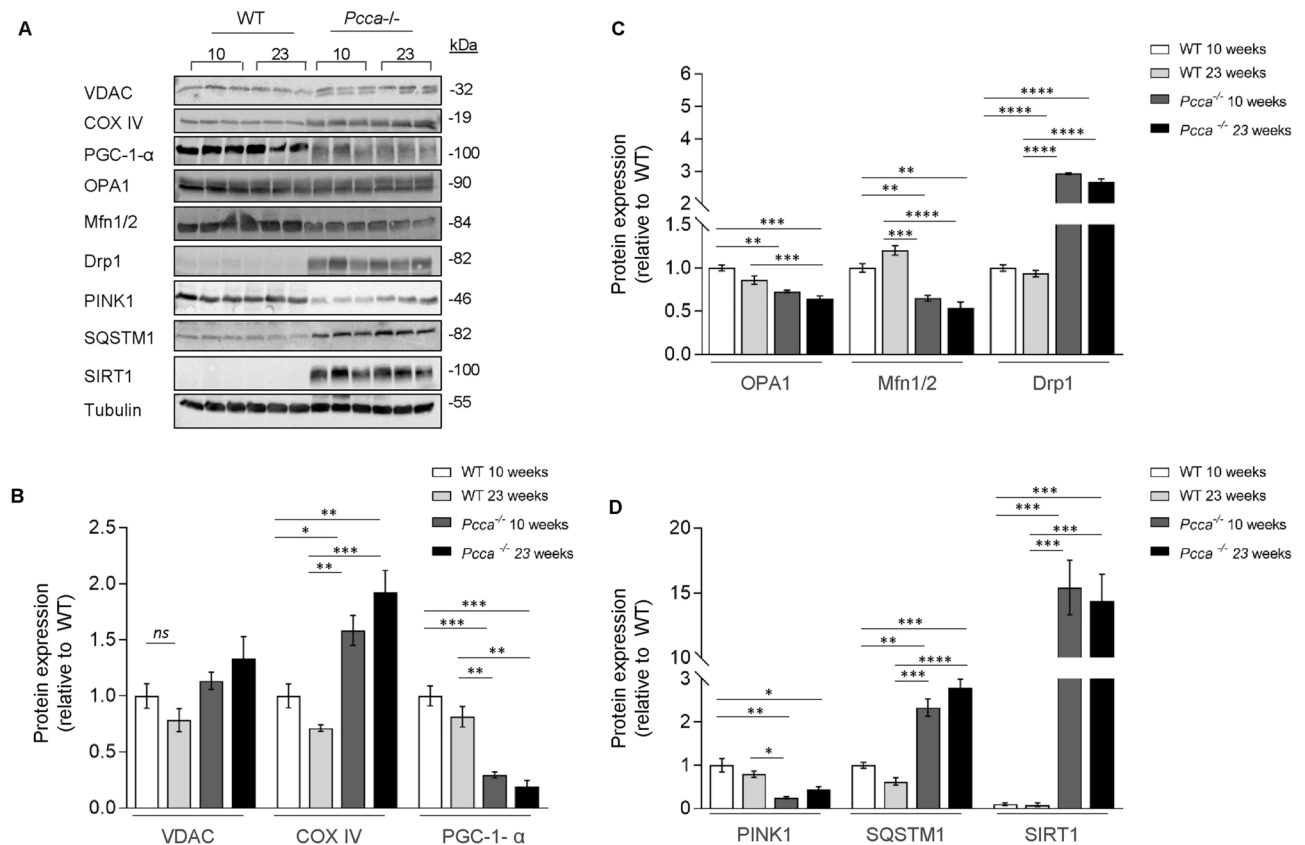


Fig. 4. Protein expression profile of 10- and 23-week-old *Pcca*^{-/-} (A138T) mice. **(A)** Immuno-blot analysis for mitochondrial homeostasis: voltage-dependent anion channel (VDAC1), cytochrome c oxidase IV (COX IV), peroxisome proliferator-activated receptor- γ coactivator-1 α (PGC-1 α); mitochondrial dynamics: optic atrophy-1 (OPA1), mitofusin1/2 (Mfn1/2), dynamin-related protein 1 (Drp1); mitochondrial quality control: sequestosome 1 (SQSTM1), PTEN-induced kinase 1 (PINK1), sirtuin1 (SIRT1). Tubulin was used as loading control. **(B)** Quantification of proteins for mitochondrial homeostasis. Data normalized to WT. n = 3 per group. **(C)** Quantification of proteins for mitochondrial dynamics. Data normalized to WT. n = 3 per group. **(D)** Quantification of proteins for mitochondrial quality control. Data normalized to WT. n = 3 per group.

mitochondrial dynamics and MQC. The identified pathways offer therapeutic intervention potential and might be targeted to rescue kidney function in future studies.

Pcca^{-/-} (A138T) mice develop CKD progressing with age, which is comparable to previously published data on renal cellular and mouse models for both PA⁸ and MMA^{7,25}. Increased biomarkers of kidney injury (KIM1, LCN2) seem to be a shared feature in both OAs and thus might have potential as follow-up parameters in patients. Human renal biopsies in OAs are scarce –especially in PA. Tubulo-interstitial nephritis is characteristic in infantile and adult MMA patients¹. However, Vernon reports focal dilatation, flattened epithelium and vacuolization in human tubular cells of an adult PA patient⁵. We detected partial flattening of tubular epithelial cells and focal tubular-cystic dilation in the kidneys of *Pcca*^{-/-} (A138T) mice. Whether these histological differences might be one explanation for earlier onset and inevitable progression to end stage renal disease in MMA compared to PA needs further investigation.

Mitochondrial networks in proximal and distal tubular segments seemed less organized and patchier in *Pcca*^{-/-} (A138T) mice highlighting the mitochondrion as target organelle in PA. Similar changes have been reported for a human renal tubular PA model⁸ and the few available patient biopsies⁵. Buchanan et al. detected that propionic acid, a key metabolite of PA, influences mitochondrial ultrastructure and dynamics in neuronal cells²⁶. Studies in murine hepatic tissue and several renal cellular MMA models confirmed ultrastructural alterations in mitochondria¹³. Investigation of a mouse model for MMA revealed a slightly different pattern with abnormally shaped mitochondria and cristae rarefaction primarily in proximal tubular cells⁷.

We detected alterations in the glutathione/thiol redox system with markedly reduced ratios of reduced to oxidized cysteine and glutathione indicating a need to counteract ROS. ROS production has been discussed as one possible pathomechanism promoting organ damage in both PA and MMA. Gallego Villar et al. reported elevated ROS levels in PA patients' fibroblasts, which were positively correlated to the severity of the mutation and apoptotic rate⁹. Deep phenotyping of the *Pcca*^{-/-} (A138T) mouse model revealed increased ROS levels in brain, heart and liver suggesting systemic ROS production and organ involvement in PA¹⁰. Isoleucine/valine load potentiated mitochondrial dysfunction in a renal cellular model for PA⁸. Anti-oxidant treatment ameliorated the

phenotype in PA patients' fibroblasts²⁷ and different cellular and animal models for MMA^{13,28} highlighting the potential impact of ROS for organ damage in both OAs. FGF21 is a highly predictive disease biomarker for mitochondrial dysfunction in MMA independent of kidney function and correlating with disease severity²⁸. We detected elevated expression levels of FGF21 progressing with age suggesting that metabolic stress response and disturbed mitochondrial function are a shared feature linking mitochondrial dysfunction to kidney damage in both OAs.

We next examined the impact of these alterations on the expression profiles of mitochondrial markers that label outer (VDAC) and inner membrane (*Sdh*, COX IV), intermembrane space (*Cyts*) and matrix (*Pdha1*). We detected increased protein levels of VDAC and COX IV as previously described for different renal PA⁸ and MMA models¹³. Transcript expression profiles of the other mitochondrial markers remained unchanged, however, an up-regulation in 40-week-old WT mice for *Sdh*, *Cyts* and *Pdha1* might suggest a relative lack in 40-week-old *Pcca*^{-/-} (*A138T*) animals. Studies in human tissue of MMA and PA patients revealed reduced activities of respiratory chain complexes and TCA cycle enzymes¹¹. We hypothesize that the up-regulation of mitochondrial markers could reflect a mechanism to compensate for deficient energy production via the RC in highly energy-dependent renal cells but cannot comment on enzyme function.

The propionate pathway provides the TCA cycle with anaplerotic fuel via succinyl-CoA¹² and energy derailment has been a matter of debate for both OAs. We observe marked elevations of α -ketoglutarate, citrate, itaconate, malate and succinate, which might be due to reduced enzymatic activity of TCA cycle enzymes. Inhibition of TCA cycle enzymes due to accumulation of disease-specific metabolites has been reported in tissues and patient cells in OAs^{11,12,29}. The TCA cycle is tightly regulated and in constant feedback with OXPHOS. OXPHOS deficiency leads to NADH accumulation with negative impact on regulatory enzymes of the TCA cycle³⁰. Both mechanisms could be involved in blocking substrate utilization in our PA model. Human renal cellular models for PA⁸ and MMA²⁵ show a similar pattern. The elevation of succinate is striking, because depletion of anaplerotic substrates has been discussed as potential pathomechanism in OAs³¹. Due to reproducibility in different human renal cellular models^{8,25}, our finding might reflect an organ-specific characteristic³².

Renal energy metabolism heavily relies on FAO fueling the TCA cycle. Impaired FAO is a feature of acute and chronic kidney disease and associated with renal fibrosis³³. Clustering of medium-chain acylcarnitines revealed a trend towards higher levels in *Pcca*^{-/-} (*A138T*) mice. We recently detected accumulation of medium and long-chain acylcarnitines in renal epithelial cells of PA and MMA patients^{8,25}. The pattern was less pronounced in the PA models and might explain why fibrosis is not a predominant feature as compared to MMA. Forny et al. described accumulation of odd chain fatty acids in the plasma of a murine MMA model³⁴ suggesting altered FAO as a shared feature in OAs. The underlying mechanisms await further investigation.

We next linked the metabolic profile to associated intracellular signaling pathways: PGC-1- α is the master regulator of MQC and controls gene expression of FAO and TCA cycle enzymes. Low levels of PGC-1- α might be responsible for the compromised performance of these players. Loss of PGC-1- α expression has been described in different renal models (e.g. diabetic kidney disease), associated with fibrosis²¹ and might be one possible explanation for CKD in PA. Multiple inductive and suppressing factors, which are active in renal injury and repair, control PGC-1- α expression and add complexity to this pathway²¹.

Mitochondria are highly dynamic networks constantly undergoing fission (Drp1) and fusion (OPA1, Mfn1/2) to adapt to environmental needs²¹. Mfn1/2 expression is positively correlated with PGC-1- α levels³⁵, while we observed a strong tendency towards mitochondrial fission in our mouse model. Kidney research identified mitochondrial fission in CKD models of more "common" cause³⁶ and might be a generalizable mechanism driving CKD of different origin.

Of note, high Drp1 levels suppress mitophagy and pharmacological Drp1 inhibition results in restauration of mitochondrial dynamics and preserves mitochondrial integrity by mitophagy initiation³⁶.

Our investigation revealed a reduction of PINK1 levels in *Pcca*^{-/-} (*A138T*) mice. We recently reported on defective mitophagy in MMA¹³ pointing towards a shared pathomechanism. Metabolic stress like protein and amino acid load further lowered already reduced PINK1 expression in a human renal MMA²⁵ model, while human renal PA cells only showed reduced PINK1 levels in high protein exposure⁸. Over-expression of PINK1 in MUT deficient cells rescued mitophagy and supported lysosomal degradation¹³. Different models of diabetic nephropathy report on low expression of PINK1 accompanied by increased mitochondrial fragmentation^{37,38}. Investigation of distinct disease entities like lung fibrosis³⁹ and neurodegenerative disorders^{40,41} revealed a similar pattern. Reduction of ROS species rescued PINK1 expression and reversed CKD³⁸. Interestingly, PGC-1- α (which is reduced in our model) exerts tissue specific effects and positively influences PINK1 expression in the kidney⁴². Activation of MQC protects against CKD of different origin⁴³. We hypothesize that PINK1 deficiency (of primary or secondary course) is a rather common disease causing mechanism. The exact mode of action is unclear. The up-regulation of the autophagy marker SQSTM1⁴⁴ might reflect a compensatory mechanism in a situation, where the removal of dysfunctional mitochondria is deficient.

Sirtuins are NAD⁺ dependent deacetylases and involved in regenerative processes such as antioxidative defence, anti-fibrotic effects and maintenance of mitochondrial function. SIRT1 is highly expressed in our model most likely to counteract the energetically and metabolically stressful conditions. SIRT1 positively regulates PGC-1- α activity through deacetylation. Strikingly, PGC-1- α is downregulated as previously observed for MMA²⁵. We hypothesize that this could be due to several factors: Since deacetylation is a reversible process, PGC-1- α could be re-acetylated by GCN5, an acetyltransferase with specific action on PGC-1- α ⁴⁵. PGC-1- α expression is negatively regulated by various other factors (e.g. GSK3- β , Akt, S6K1, ubiquitin proteasome)^{45,46}. GSK3- β mediated phosphorylation and proteasomal degradation of PGC-1- α have been described in mice as a response against oxidative stress³⁹. Epigenetic modifications block PGC-1- α at the transcription level or via demethylation. Transcription factors like HES1 have been inversely associated with PGC-1- α expression in human kidney and metabolic disease^{45,46}. Finally, PGC-1- α expression relies on numerous environmental factors⁴⁷. The complexity

of possible influencing factors warrants further investigation, particularly since influencing PGC-1- α expression might be a promising therapeutic target.

Our study has several limitations. Due to the limited accessibility of the material, we examined molecular signatures in renal tissue only and the number of animals per group is rather small and the data need larger-scale confirmation. Only female mice developed a renal phenotype. Sex specific disease susceptibility has been reported in mouse models for MMA^{7,34} and been observed for both male and female mice. Different mouse strains and methods of genetic manipulation might be a reason. We cannot draw conclusions on the systemic effects of CKD on circulating metabolites in plasma and urine. The kidney extracts represent a blend of multiple cell types, and therefore, we cannot comment on individual contributions of different cell types to the renal phenotype. The relevance of the histopathological findings in mice for onset and progression of human CKD is unclear. All mentioned points warrant further investigation in future studies.

In sum, this study confirms disturbed mitochondrial homeostasis and MQC as potential CKD-driving mechanisms in PA and highlights the mitochondrion as target organelle for CKD development in OAs. The analysis sheds new light on pharmacologically targetable aims like the modulation of mitochondrial biogenesis using AMPK activators (e.g. metformin, AICAR), mitophagy/autophagy pathways (e.g. Tat-beclin1, resveratrol)^{21,47} or mitochondrial dynamics (e.g. mitochondrial division inhibitor 1). The evaluation of their therapeutic potential awaits further investigation.

Material and methods

Mice handling and isolation of kidneys

Mice kidneys used in this study were kindly provided by Prof. Dr. M. A. Barry (Mayo Clinic, Minnesota, US, generation of the model) and Prof. Dr. L.R. Desviat (Centro de Biología Molecular Severo Ochoa, Universidad Autónoma, Madrid, Spain, animal husbandry). The mouse model has been thoroughly characterized⁴⁸.

All animal studies were approved by the Institutional Ethical Committee for Animal Experimentation (Universidad Autónoma de Madrid, reference CEI 963-A026 and CEI-134-2830) and by the Regional Environment Department (Comunidad de Madrid, reference PROEX 194/19). Animal housing and maintenance protocols followed the local authority guidelines. Mice were maintained on standard chow. All the experiments were carried out in a pathogen-free environment at the animal facility of the Centro de Biología Molecular Severo Ochoa, in accordance with the Spanish Law of Animal Protection. Food and water were available ad libitum, and mice were maintained in a temperature-controlled environment on a 12/12 h light–dark cycle. All mice used, wild-type (WT^{+/+}) and hypomorphic *Pcca*^{-/-} (A138T), were females (4-, 10-, 23- and 40-week-old) in a C57BL/6 background. *Pcca*^{-/-} (A138T) mice were obtained by crossing *Pcca*^{-/-} male with *Pcca*^{+/+} female mice to increase the number of *Pcca*^{-/-} animals. At the time/age stated for each experiment, mice were sacrificed in a carbon dioxide chamber and perfused with 50 mL of NaCl. Immediately after, kidneys were surgically excised. One kidney was snap-frozen in liquid nitrogen for RNA and protein extraction and stored at -80 °C, and the other was immersed in 4% PFA overnight and stored at 4 °C.

In order to obtain serum specimens, whole blood was collected by cardiac puncture and transferred to an Eppendorf tube. The blood samples were left for 1 h at 37 °C and at 4 °C overnight to facilitate coagulation, followed by two consecutive centrifugation steps (1200 × g, 5 min, and 4 °C) after which the respective supernatants were collected. The isolated serum fractions were stored at -80 °C.

Blood analysis was performed using the following kit according to the manufacturer's instructions: Blood urea nitrogen (BUN): LT-UR; Labor&Technik, Eberhard Lehmann GmbH.

RNA extraction

RNA was extracted from frozen kidneys of female WT and *Pcca*^{-/-} (A138T) mice (4-week-, 23-week and 40-week-old animals) to study mRNA levels using real-time quantitative PCR. The total RNA extraction was carried out with the RNeasy Mini Kit (Qiagen, cat. no. 74104). For disruption of the tissue, a mortar and pestle were used. The tissue was frozen in liquid nitrogen and grinded to a fine powder under liquid nitrogen. The suspension was transferred to a new tube and mixed with 600 µl of lysis buffer. Homogenization was performed with QIAshredder columns (Qiagen, cat. no. 79654) by pipetting the lysate directly into a QIAshredder spin column and centrifuging for 2 min at full speed. After centrifugation (3 min at full speed), 70% ethanol was added to the flowthrough, and it was carefully mixed by pipetting. 700 µl of the sample were transferred to the RNeasy spin column and centrifuged for 15 s at 8000 × g. The column was washed with 700 µl RW1 buffer and centrifuged for 15 s at 8000 × g, followed by two subsequent washes with 500 µl RPE buffer and centrifugation at 8000 × g for 15 s and 2 min, respectively. The column was placed in a new collection tube and centrifuged for 2 min at 8000 × g. The RNA was eluted in 30 µl RNase-free water by centrifuging for 1 min at 8000 × g.

Reverse transcription to cDNA

For reverse transcription of mRNA, the First Strand cDNA Synthesis Kit (Thermo Fisher Scientific, catalog number K1612) was used. If RNA yields were sufficient, 2 µg of RNA was utilized. The RNA, diluted in RNase-free water, was mixed with oligo(dT)₁₈ primer and random hexamer primer (0.5 µl each) to a final volume of 11 µl. This mixture was incubated at 65 °C for 5 min and then placed on ice for at least 1 min.

A cDNA synthesis mix was then prepared, consisting of: 4 µl of 5 × Reaction Buffer, 1 µl of RiboLock RNase Inhibitor (20 U/µl), 2 µl of 10 mM dNTP mix, and 2 µl of M-MuLV Reverse Transcriptase (20 U/µl). A total of 9 µl of this cDNA synthesis mix was added to the RNA/primer mixture, gently mixed, briefly centrifuged, and incubated for 5 min at 25 °C, followed by 60 min at 37 °C. The reaction was terminated at 70 °C for 5 min and then chilled on ice.

Real-time quantitative PCR

For real-time qPCR, the CFX96 Real-Time System (Bio-Rad Laboratories) with SYBR green labeling was used. The cDNA was diluted 1:10 in RNase-free water for the qPCR. A reaction mix was prepared containing 4 µl of SYBR Green iQ SuperMix (Bio-Rad Laboratories, catalog number 1708860), 0.5 µl of forward primer, 0.5 µl of reverse primer, and 5 µl of diluted cDNA. GAPDH served as the reference gene. Each well of a 96-well plate (Bio-Rad Laboratories, catalog number HSP9601) was filled with 10 µl of the reaction mix, and the plate was sealed with optical adhesive film. The real-time cyclers was set up with an initial PCR activation step of 3 min at 95 °C, followed by 44 cycles of a 3-step program: 20 s at 95 °C for denaturation, 30 s at 58 °C for annealing, and 40 s at 72 °C for extension. Primer specificity for the detected product was confirmed by melt-curve analysis. The primers used were:

Gene	Forward	Reverse
<i>Gapdh</i>	CCCATCACCATCTTCCAG	ATGACCTTGCCCACAGCC
<i>Cycs</i>	CCAAATCTCCACGGTCTGTTC	ATCAGGGTATCTCTCCCCAG
<i>Fgf21</i>	CTGCTGGGGGTCTACCAAG	CTGCGCCTACCACTGTTC
<i>Havcr1</i>	ACATATCGTGGAATCACAACGAC	ACAAGCAGAAGATGGGCATTG
<i>Lcn2</i>	TGGCCCTGAGTGTCATGTG	CTCTTGTAAGCTCATAGATGGTGC
<i>Pdha1</i>	GAAATGTGACCTTCATCGGCT	TGATCCGCCTTTAGCTCCATC
<i>Sdh</i>	GGAACACTCCAAAACAGACCT	CCACCACTGGGTATTGAGTAGAA

Immuno-blotting

RIPA buffer was supplied with EDTA-free protease inhibitor cocktail (cOmplete, Roche, # 11697498001) and phosphatase inhibitor (PhosSTOP, Roche, # 0490683701). 100 mg renal tissue was grinded on ice with 800 µl of complete RIPA buffer for 1 min. The sample was centrifuged at 16,000×g at 4 °C for 15 min and the supernatant collected. BCA assay (Pierce, Thermo Fisher Scientific) was used to determine the protein concentration. Samples were loaded using 100 µg protein/lane. SDS-PAGE was used for protein separation followed by blotting on a nitrocellulose membrane. Blocking was performed with 5% non-fat milk. The membranes were probed with the respective antibodies at 4 °C for 12 h, followed by incubation with the peroxidase-tagged secondary antibody (20 °C, 2 h) and developed using chemiluminescence (WBKLS0050, Millipore, Life technologies). γ-tubulin was used for protein normalization. Image J software (Image J 2.0.0-rc-68/1.52 g; Java 1.8.0_172 [64-bit]; <https://imagej.net/ij/>) was used to quantify the density of each signal using for protein normalization.

Antibodies used for immuno-blotting

Anti-PINK1 (1:400), ab23707, rabbit polyclonal (Abcam); anti-SQSTM1 (1:400), abMBL PM045, rabbit polyclonal (MBL International Corporation); anti-VDAC (1:1000), ab4661, rabbit monoclonal (Cell Signaling Technology); anti-DRP1 (1:200), rabbit monoclonal, ab8570 (Cell Signaling Technology); Anti-Lipocalin-2 (1:400), ab63929, rabbit polyclonal IgG antibody (Abcam), anti-OPA1 (1:500) rabbit monoclonal, ab80471 (Cell signaling Technology); anti-SIRT1 (1:500), rabbit polyclonal, ab2310 (Cell Signaling Technology), anti-COX IV (1:500), ab14744, mouse monoclonal (Abcam); anti-PGC1-α (1:500), ab19838, rabbit polyclonal (Abcam); anti-Mitofusin1/2 (1:1000), ab57602, mouse monoclonal (Abcam); anti-gamma-Tubulin (1:1000), ab T5326, mouse monoclonal (Sigma).

Quantitative profiling of metabolites by liquid chromatography and mass spectrometry (LC-MS/MS)

Murine renal tissue biopsies were thawed and homogenised with ice-cold PBS supplemented with 1% protease inhibitor cocktail (Sigma Nr. P8340-5 mL), using a cordless pestle motor and disposable pellet mixers (VWR Nr. 47747-366). Buffer volume was adjusted such to reach a target of 0.1 to 0.3 mg wet-tissue/mL lysis buffer. Whole tissue homogenates were aliquoted for downstream measurement of total protein concentration, flash-frozen and stored at −80 °C. All metabolites as well as creatinine and the redox thiol pools were determined according to a previously published procedure⁵⁰. Lactate, TCA and glycolysis intermediates and other organic acids, and folates were determined as described in previous work⁵¹. Amino acids and neurotransmitters were determined using a previously described protocol^{52,53}. A commercially available standardized amino acid mixture was utilized to generate a calibration curve for amino acids (Amino acid standards, physiological, Sigma, Nr. A9906-10 mL). Calibration curves for all other metabolites were prepared from individual stock solutions prepared in house. Quantitation accuracy was examined by monitoring homocysteine and methylmalonic acid concentrations in an external quality control, namely, the Control Special Assays in Serum, European Research Network for the evaluation and improvement of screening, diagnosis, and treatment of Inherited disorders of Metabolism (ERNDIM) IQCS, SAS-02.1 and SAS-02.2 from MCA Laboratories, Winterswijk, Netherlands. For all other metabolites, quantitation trueness was tested by examining metabolite concentrations in plasma from a previously validated sample isolated from a healthy control individual with respect to standard reference ranges, using the same calibration curves and LC-MS/MS running conditions. Quantification of metabolites was carried out with Analyst 1.7.2 software, 2022 AB Sciex (<https://sciex.com/products/software/analyst-software>).

Transmission electron microscopy

Mice were sacrificed in a carbon dioxide chamber and perfused through the left ventricle with with 50 mL of NaCl and then with a solution of 4% formaldehyde and 2% glutaraldehyde in 0.1 M phosphate buffer pH

7.4. Kidneys were postfixed in the same solution for 2 h at room temperature and overnight at 4 °C. Upper kidney pole was cut into transverse slabs that were postfixed in 1% osmium tetroxide in 0.1 M cacodylate buffer, dehydrated in ethanol and embedded in Epon-Araldite. Serial ultrathin sections of transverse section of kidneys were collected on pioloform-coated, single-hole grids, and stained with uranyl acetate and lead citrate. The sections were analysed with a JEM-1010 transmission electron microscope (Jeol, Japan) equipped with a side-mounted CCD camera Mega View III from Olympus Soft Imaging System GmbH (Muenster, Germany, <https://www.olympus-lifescience.com>). Mitochondria of 40-week-old mice were sampled randomly in the distal and proximal tubules of the kidney at a magnification of 3000X.

Statistical analysis

Data represent mean \pm SEM. Data were first tested with an F test to compare variances. More than 2 groups were compared with ANOVA using Tukey's correction; in the cases where variances among the groups were significantly different, Browne-Forsythe and Welch ANOVA test with Dunnett's test was used. GraphPad Prism 9 software (<https://www.graphpad.com>) was used for the analyses. * $P < 0.05$, ** $P < 0.01$, *** $P < 0.001$, and **** $P < 0.0001$; ns: not significant. Quantitative analysis (metabolite concentrations in tissue nmol/mg protein) are summarized in the supplementary. All values are displayed as compared to WT.

Data availability

The datasets reported are available upon reasonable request to the corresponding author.

Received: 7 March 2024; Accepted: 11 November 2024

Published online: 16 December 2024

References

1. Forny, P. et al. Guidelines for the diagnosis and management of methylmalonic acidemia and propionic acidemia: First revision. *J. Inherit. Metab. Dis.* **44**, 566–592. <https://doi.org/10.1002/jimd.12370> (2021).
2. Quintero, J. et al. The role of liver transplantation in propionic Acidemia. *Liver Transpl.* **24**, 1736–1745. <https://doi.org/10.1002/lt.25344> (2018).
3. Charbit-Henrion, F. et al. Early and late complications after liver transplantation for propionic Acidemia in children: a two centers study. *Am. J. Transplant.* **15**, 786–791. <https://doi.org/10.1111/ajt.13027> (2015).
4. Shchelochkov, O. A. et al. Chronic kidney disease in propionic Acidemia. *Genet. Med.* **21**, 2830–2835. <https://doi.org/10.1038/s41436-019-0593-z> (2019).
5. Vernon, H. J., Bagnasco, S., Hamosh, A. & Sperati, C. J. Chronic kidney disease in an adult with propionic acidemia. *JIMD Rep.* **12**, 5–10. https://doi.org/10.1007/8904_2013_237 (2014).
6. Dao, M. et al. Long-term renal outcome in Methylmalonic Acidzemia in adolescents and adults. *Orphanet. J. Rare Dis.* **16**, 220. <https://doi.org/10.1186/s13023-021-01851-z> (2021).
7. Manoli, I. et al. Targeting proximal tubule mitochondrial dysfunction attenuates the renal disease of methylmalonic acidemia. *Proc. Natl. Acad. Sci. USA* **110**, 13552–13557. <https://doi.org/10.1073/pnas.1302764110> (2013).
8. Schumann, A. et al. Mitochondrial damage in renal epithelial cells is potentiated by protein exposure in propionic aciduria. *J. Inherit. Metab. Dis.* **44**, 1330–1342. <https://doi.org/10.1002/jimd.12419> (2021).
9. Gallego-Villar, L. et al. Functional characterization of novel genotypes and cellular oxidative stress studies in propionic Acidemia. *J. Inherit. Metab. Dis.* **36**, 731–740. <https://doi.org/10.1007/s10545-012-9545-3> (2013).
10. Gallego-Villar, L. et al. In vivo evidence of mitochondrial dysfunction and altered redox homeostasis in a genetic mouse model of propionic Acidemia: Implications for the pathophysiology of this disorder. *Free Radic. Biol. Med.* **96**, 1–12. <https://doi.org/10.1016/j.freeradbiomed.2016.04.007> (2016).
11. de Keyzer, Y. et al. Multiple OXPHOS deficiency in the liver, kidney, heart, and skeletal muscle of patients with methylmalonic aciduria and propionic aciduria. *Pediatr. Res.* **66**, 91–95. <https://doi.org/10.1203/PDR.0b013e3181a7c270> (2009).
12. Dimitrov, B. et al. Organic acidurias: Major gaps, new challenges, and a yet unfulfilled promise. *J. Inherit. Metab. Dis.* **44**, 9–21. <https://doi.org/10.1002/jimd.12254> (2021).
13. Luciani, A. et al. Author Correction: Impaired mitophagy links mitochondrial disease to epithelial stress in methylmalonyl-CoA mutase deficiency. *Nat. Commun.* **11**, 1719. <https://doi.org/10.1038/s41467-020-15565-6> (2020).
14. Head, P. E. et al. Aberrant methylmalonylation underlies methylmalonic acidemia and is attenuated by an engineered sirtuin. *Sci. Transl. Med.* **14**, eabn4772. <https://doi.org/10.1126/scitranslmed.abn4772> (2022).
15. Broeks, M. H., van Karnebeek, C. D. M., Wanders, R. J. A., Jans, J. J. M. & Verhoeven-Duif, N. M. Inborn disorders of the malate aspartate shuttle. *J. Inherit. Metab. Dis.* **44**, 792–808. <https://doi.org/10.1002/jimd.12402> (2021).
16. Beach, T. E. et al. Targeting succinate dehydrogenase with malonate ester prodrugs decreases renal ischemia reperfusion injury. *Redox Biol.* **36**, 101640. <https://doi.org/10.1016/j.redox.2020.101640> (2020).
17. Jang, C. et al. Metabolite exchange between mammalian organs quantified in pigs. *Cell Metab.* **34**, 1410. <https://doi.org/10.1016/j.cmet.2022.08.006> (2022).
18. Afshinnia, F. et al. Impaired beta-oxidation and altered complex lipid fatty acid partitioning with advancing CKD. *J. Am. Soc. Nephrol.* **29**, 295–306. <https://doi.org/10.1681/ASN.2017030350> (2018).
19. Longo, N., Sass, J. O., Jurecka, A. & Vockley, J. Biomarkers for drug development in propionic and methylmalonic acidemias. *J. Inherit. Metab. Dis.* **45**, 132–143. <https://doi.org/10.1002/jimd.12478> (2022).
20. Anzmann, A. F. et al. Multi-omics studies in cellular models of methylmalonic acidemia and propionic acidemia reveal dysregulation of serine metabolism. *Biochim. Biophys. Acta Mol. Basis Dis.* **1865**, 165538. <https://doi.org/10.1016/j.bbadis.2019.165538> (2019).
21. Tang, C. et al. Mitochondrial quality control in kidney injury and repair. *Nat. Rev. Nephrol.* **17**, 299–318. <https://doi.org/10.1038/s41581-020-00369-0> (2021).
22. Giacomello, M., Pyakurel, A., Glytsou, C. & Scorrano, L. The cell biology of mitochondrial membrane dynamics. *Nat. Rev. Mol. Cell Biol.* **21**, 204–224. <https://doi.org/10.1038/s41580-020-0210-7> (2020).
23. Klionsky, D. J. et al. Autophagy in major human diseases. *EMBO J* **40**, e108863 (2021).
24. Bhargava, P. & Schnellmann, R. G. Mitochondrial energetics in the kidney. *Nat. Rev. Nephrol.* **13**, 629–646. <https://doi.org/10.1038/nrneph.2017.107> (2017).
25. Schumann, A. et al. The impact of metabolic stressors on mitochondrial homeostasis in a renal epithelial cell model of methylmalonic aciduria. *Sci. Rep.* **13**, 7677. <https://doi.org/10.1038/s41598-023-34373-8> (2023).
26. Buchanan, E. et al. Propionic acid induces alterations in mitochondrial morphology and dynamics in SH-SY5Y cells. *Sci. Rep.* **13**, 13248. <https://doi.org/10.1038/s41598-023-40130-8> (2023).

27. Gallego-Villar, L., Perez, B., Ugarte, M., Desviat, L. R. & Richard, E. Antioxidants successfully reduce ROS production in propionic acidemia fibroblasts. *Biochem. Biophys. Res. Commun.* **452**, 457–461. <https://doi.org/10.1016/j.bbrc.2014.08.091> (2014).
28. Manoli, I. et al. FGF21 underlies a hormetic response to metabolic stress in methylmalonic acidemia. *JCI Insight* <https://doi.org/10.1172/jci.insight.124351> (2018).
29. Morath, M. A. et al. Neurodegeneration and chronic renal failure in methylmalonic aciduria—a pathophysiological approach. *J. Inherit. Metab. Dis.* **31**, 35–43. <https://doi.org/10.1007/s10545-007-0571-5> (2008).
30. Martínez-Reyes, I. & Chandel, N. S. Mitochondrial TCA cycle metabolites control physiology and disease. *Nat. Commun.* **11**, 102. <https://doi.org/10.1038/s41467-019-13668-3> (2020).
31. Forny, P. et al. Integrated multi-omics reveals anaplerotic rewiring in methylmalonyl-CoA mutase deficiency. *Nat. Metab.* **5**, 80–95. <https://doi.org/10.1038/s42255-022-00720-8> (2023).
32. He, W., Wang, Y., Xie, E. J., Barry, M. A. & Zhang, G. F. Metabolic perturbations mediated by propionyl-CoA accumulation in organs of mouse model of propionic acidemia. *Mol. Genet. Metab.* **134**, 257–266. <https://doi.org/10.1016/j.ymgme.2021.09.009> (2021).
33. Aranda-Rivera, A. K., Cruz-Gregorio, A., Aparicio-Trejo, O. E. & Pedraza-Chaverri, J. Mitochondrial redox signaling and oxidative stress in kidney diseases. *Biomolecules* <https://doi.org/10.3390/biom11081144> (2021).
34. Forny, P. et al. Novel mouse models of methylmalonic aciduria recapitulate phenotypic traits with a genetic dosage effect. *J. Biol. Chem.* **291**, 20563–20573. <https://doi.org/10.1074/jbc.M116.747717> (2016).
35. Lynch, M. R., Tran, M. T. & Parikh, S. M. PGC1alpha in the kidney. *Am. J. Physiol. Renal Physiol.* **314**, F1–F8. <https://doi.org/10.1152/ajprenal.00263.2017> (2018).
36. Galvan, D. L., Green, N. H. & Danesh, F. R. The hallmarks of mitochondrial dysfunction in chronic kidney disease. *Kidney Int.* **92**, 1051–1057. <https://doi.org/10.1016/j.kint.2017.05.034> (2017).
37. Zhan, M., Usman, I. M., Sun, L. & Kanwar, Y. S. Disruption of renal tubular mitochondrial quality control by Myo-inositol oxygenase in diabetic kidney disease. *J. Am. Soc. Nephrol.* **26**, 1304–1321. <https://doi.org/10.1681/ASN.2014050457> (2015).
38. Xiao, L. et al. The mitochondria-targeted antioxidant MitoQ ameliorated tubular injury mediated by mitophagy in diabetic kidney disease via Nrf2/PINK1. *Redox Biol.* **11**, 297–311. <https://doi.org/10.1016/j.redox.2016.12.022> (2017).
39. Bueno, M. et al. PINK1 deficiency impairs mitochondrial homeostasis and promotes lung fibrosis. *J. Clin. Invest.* **125**, 521–538. <https://doi.org/10.1172/JCI74942> (2015).
40. Du, F. et al. PINK1 signalling rescues amyloid pathology and mitochondrial dysfunction in Alzheimer's disease. *Brain* **140**, 3233–3251. <https://doi.org/10.1093/brain/awx258> (2017).
41. Moraes, V. A. et al. Parkinson's disease mutations in PINK1 result in decreased Complex I activity and deficient synaptic function. *EMBO Mol. Med.* **1**, 99–111. <https://doi.org/10.1002/emmm.200900006> (2009).
42. Qian, L. et al. Peroxisome proliferator-activated receptor gamma coactivator-1 (PGC-1) family in physiological and pathophysiological process and diseases. *Signal Transduct. Target Ther.* **9**, 50. <https://doi.org/10.1038/s41392-024-01756-w> (2024).
43. Bhatia, D. & Choi, M. E. The emerging role of mitophagy in kidney diseases. *J. Life Sci. (Westlake Village)* **1**, 13–22 (2019).
44. Dikic, I. & Elazar, Z. Mechanism and medical implications of mammalian autophagy. *Nat. Rev. Mol. Cell Biol.* **19**, 349–364. <https://doi.org/10.1038/s41580-018-0003-4> (2018).
45. Choi, J. et al. Potential roles of PINK1 for increased PGC-1alpha-mediated mitochondrial fatty acid oxidation and their associations with Alzheimer disease and diabetes. *Mitochondrion* **18**, 41–48. <https://doi.org/10.1016/j.mito.2014.09.005> (2014).
46. Huang, C., Bian, J., Cao, Q., Chen, X. M. & Pollock, C. A. The mitochondrial kinase PINK1 in diabetic kidney disease. *Int. J. Mol. Sci.* <https://doi.org/10.3390/ijms22041525> (2021).
47. Fontecha-Barriuso, M. et al. The role of PGC-1alpha and mitochondrial biogenesis in kidney diseases. *Biomolecules* <https://doi.org/10.3390/biom10020347> (2020).
48. Guenzel, A. J. et al. Generation of a hypomorphic model of propionic acidemia amenable to gene therapy testing. *Mol. Ther.* **21**, 1316–1323. <https://doi.org/10.1038/mt.2013.68> (2013).
49. Schneider, C. A., Rasband, W. S. & Eliceiri, K. W. NIH image to ImageJ: 25 years of image analysis. *Nat. Methods* **9**, 671–675. <https://doi.org/10.1038/nmeth.2089> (2012).
50. Behringer, S. et al. Targeted metabolic profiling of methionine cycle metabolites and redox thiol pools in mammalian plasma, Cells and Urine. *Metabolites* <https://doi.org/10.3390/metabo9100235> (2019).
51. Hannibal, L. et al. Metabolic profiling in human fibroblasts enables subtype clustering in glycogen storage disease. *Front Endocrinol. (Lausanne)* **11**, 579981. <https://doi.org/10.3389/fendo.2020.579981> (2020).
52. Maier, J. P. et al. Inhibition of metabotropic glutamate receptor III facilitates sensitization to alkylating chemotherapeutics in glioblastoma. *Cell Death Dis.* **12**, 723. <https://doi.org/10.1038/s41419-021-03937-9> (2021).
53. Moritz, L., Klotz, K., Grunert, S. C., Hannibal, L. & Spiekerkoetter, U. Metabolic phenotyping in phenylketonuria reveals disease clustering independently of metabolic control. *Mol. Genet. Metab.* **138**, 107509. <https://doi.org/10.1016/j.ymgme.2023.107509> (2023).

Acknowledgements

The authors thank Ilona Skatulla for excellent technical assistance.

Author contributions

A.S.: study design, execution of experiments, data interpretation, supervised the study, preparation of manuscript. A.M.: execution of experiments, E.R.: execution of experiments, A.L.K.: execution of experiments, K.A.Z.: execution of experiments, C.S.: interpretation of histological data, S.T.: commented on the paper, O.S.: commented on the paper, M.B.: collaboration on animal model, B.N.: execution of experiments, M.K.: planning and analysis of experiments, L.H.: generation of metabolomics data, L.R.D.: collaboration on animal model, U.S.: supervised the study. All authors revised the manuscript.

Funding

This study was supported by the Division of Inborn Errors of Metabolism at the Department of Pediatrics, Adolescent Medicine and Neonatology Freiburg and by the Freiburg Center for Rare Diseases. AS and MK were funded by the Deutsche Forschungsgemeinschaft (DFG, German Research Foundation) Project-ID 431984000—CRC 1453 Nephrogenetics. AS was supported by the Research Commission of the Faculty of Medicine at the University of Freiburg (SCHU2175/21) and by the Berta-Ottenstein-Programme for Advanced Clinician Scientists, Faculty of Medicine, University of Freiburg. MK was supported by Germany's Excellence Strategy (CIBSS, EXC-2189, project ID 390939984). KAZ was supported by the Berta-Ottenstein-Programme for Clinician Scientists, Faculty of Medicine, University of Freiburg. The Proteomic Platform—Core Facility was supported by the Medical Faculty of the University of Freiburg to O.S. (2021/A3-Sch). The Translational Metabolomics Core

Facility was supported by the Faculty of Medicine, University Hospital Freiburg to LH and US. (Grant Nr. 2023/A7-Han). The research performed in Madrid was funded by Spanish Ministry of Science and Innovation and European Regional Development Fund (Grants PID2019-105344RB-I00/AEI/<https://doi.org/10.13039/501100011033> and PID2022-137238OB-I00) and by Fundación Ramón Areces (grant from XX National Call 2020).

Open Access funding enabled and organized by Projekt DEAL.

Declarations

Competing interests

The authors declare no competing interests.

Ethical approval

No material of human origin was used in this publication.

Human and animal rights

All animal studies were approved by the Institutional Ethical Committee for Animal Experimentation (Universidad Autónoma de Madrid, references CEI 963-A026 and CEI-134-2830) and by the Regional Environment Department (Comunidad de Madrid, reference PROEX 194/19 and PROEX 204.5/24). The work with mice was performed in accordance with the ARRIVE guidelines (approval number PROEX 194-2019 and PROEX 204.5/24). Animal housing and maintenance protocols followed the local authority guidelines.

Additional information

Supplementary Information The online version contains supplementary material available at <https://doi.org/10.1038/s41598-024-79572-z>.

Correspondence and requests for materials should be addressed to A.S.

Reprints and permissions information is available at www.nature.com/reprints.

Publisher's note Springer Nature remains neutral with regard to jurisdictional claims in published maps and institutional affiliations.

Open Access This article is licensed under a Creative Commons Attribution 4.0 International License, which permits use, sharing, adaptation, distribution and reproduction in any medium or format, as long as you give appropriate credit to the original author(s) and the source, provide a link to the Creative Commons licence, and indicate if changes were made. The images or other third party material in this article are included in the article's Creative Commons licence, unless indicated otherwise in a credit line to the material. If material is not included in the article's Creative Commons licence and your intended use is not permitted by statutory regulation or exceeds the permitted use, you will need to obtain permission directly from the copyright holder. To view a copy of this licence, visit <http://creativecommons.org/licenses/by/4.0/>.

© The Author(s) 2024